submitted to *Werkst. Korros.*, 3/96

The Oxidation Behavior of ODS Iron Aluminides

B. A. Pint, P. F. Tortorelli and I. G. Wright

Oak Ridge National Laboratory,
P. O. Box 2008,
Oak Ridge, TN 37831-6156

Abstract

Oxide-dispersed Fe-28at.%Al-2%Cr alloys were produced by a powder metallurgy technique followed by hot extrusion. A variety of stable oxides were added to the base alloy to assess the effect of these dopants on the oxidation behavior at 1200°C in air and O_2. An Al_2O_3 dispersion flattened the α-Al_2O_3 scale, but produced none of the other reactive element effects and had an adverse influence on the long-term oxidation behavior. A Y_2O_3 dispersion improved the alumina scale adhesion relative to a Zr alloy addition at 1200° and 1300°C. However, the Y_2O_3 dispersion was not as effective in improving scale adhesion in Fe_3Al as it is in FeCrAl. This inferior performance is attributed to a larger amount of interfacial void formation on ODS Fe_3Al.

Introduction

Interest in advanced power generation cycles that involve indirectly-fired gas turbines, in which coal- or gas-fired high-temperature heat exchangers are used to heat a working fluid in a closed system, has led to interest in materials for heat exchangers

capable of operation at temperatures of the order of 1200 to 1300°C. The candidate materials are ceramics and, possibly, oxide dispersion-strengthened (ODS) alloys. An ODS FeCrAl alloy met the strength requirements for such an application, in which the working fluid at 0.9 MPa was heated from 800 to 1100°C over a tube length of 4m [1].

The oxidation life of ODS FeCrAl alloys is determined by their ability to form or reform a protective alumina scale, and can be related to the time required for the aluminum content of the alloy to be depleted to some minimum level [2-5]. As a result, the service life is a function of the available aluminum content of the alloys and the minimum aluminum level at which breakaway oxidation occurs. Therefore, there is a minimum cross sectional thickness which can be safely employed at temperatures above 1200°C. The major factors that result in depletion of the reservoir of aluminum in the alloy are the inherent growth rate of the aluminum oxide; and the tendency for the scale to spall, which results in a (temporary) increase in oxide growth rate in the area affected by spallation. Because of their significantly higher aluminum content (≥28 at% compared to ≈9 at%), alloys based on Fe_3Al afford a potentially larger reservoir of aluminum to sustain oxidation resistance at higher temperatures and, therefore, offer a possible improvement over the currently-available ODS FeCrAl alloys [6].

Iron aluminides possess excellent high temperature (800-1300°C) corrosion resistance[7-11] but at these temperatures they do not have sufficient strength for structural applications[9,12,13]. Two possible solutions are to use them as coatings [14,15] and to develop a means of strengthening the alloy at high temperatures [12].

Conventional alloying approaches have not been successful in retaining the strength levels necessary for high temperature applications, and thus current efforts are focused on oxide dispersion strengthening to improve the creep strength at 800°C-1200°C [13].

Oxide dispersions offer an excellent opportunity to improve both the mechanical properties and the oxidation resistance by the addition of a reactive element (RE) oxide such as Y_2O_3. (Commercial ODS alloys typically contain a mixed Y_2O_3-Al_2O_3 dispersion [16-18].) Previous work [10,11,19] has shown that RE alloy additions (Y or Zr) are effective in improving the oxidation resistance of iron aluminides at temperatures above 900°C and a similar improvement is expected for the addition of an RE oxide dispersion. The use of RE oxide dispersions has improved the oxidation resistance of various Al_2O_3-forming alloys such as FeCrAl [1-5,18,20,21], NiCrAl [22,23] and NiAl [24,25]. The present paper examines the effects of several different oxide additions on the oxidation behavior of a base Fe-28at%Al-2%Cr (FAS) alloy. A comparison is made among cast, RE-doped FAS, Al_2O_3-dispersed FAS and RE oxide-dispersed FAS. Initial comparisons of ODS Fe_3Al to cast Fe_3Al showed that there was little or no difference in performance at temperatures below 1000°C [26]. Thus this work has focused on higher temperatures, particularly 1200° and 1300°C.

Experimental Procedure

Gas-atomized Fe-28%Al-2%Cr [27] powder and sub-micron oxide powder were mechanically blended in a flowing Ar atmosphere using a water-cooled, high-speed attritor and stainless steel balls.

Standard dopant additions of 0.2cation% were made. FAS powder was milled without any addition to create an Al_2O_3 dispersion. The blended powder was canned, degassed, and extruded at 1100°C. For comparison, a FAS powder extrusion without an oxide addition, cast FAS, cast Fe-28%Al-5%Cr-0.1%Zr (FAL), cast β-NiAl (with and without a 0.04% Zr addition), and a commercial ZrO_2-dispersed (0.06%Zr) Fe-20.4%Cr-10.6%Al alloy (Kanthal alloy APM) were also tested. Chemical compositions are given in Table I. Scanning electron microscopy (SEM) and transmission electron microscopy (TEM) of the as-extruded alloys consistently showed a $\approx 1\mu m$ grain size and a bimodal particle distribution of 20-50nm particles within grains and $0.2\text{-}1\mu m$ particles at grain boundaries. The number of larger particles generally increased with oxygen content.

Oxidation coupons (10-15 mm diameter x 1 mm thick) were polished to a 0.3 μm finish with alumina powder and ultrasonically cleaned in acetone and methanol prior to oxidation. Isothermal oxidation experiments were conducted in 1 atm dry, flowing O_2 with weight gains measured by a Cahn model 1000 microbalance. Cyclic oxidation experiments were conducted at 1200°C and 1300°C in air and in dry, flowing O_2. In short-term cyclic testing (2h cycles), specimens were hung in a furnace with dry, flowing O_2 and weight changes were measured continuously using a Cahn model 1000 microbalance to check for any indication of isothermal spallation. (In these tests, spallation was only observed upon cooling.) During long-term testing (100h cycles), specimens were placed in the furnace in pre-annealed alumina crucibles so that spalled oxide could be collected and weighed. In both types of cyclic tests, the specimen

weight changes were measured before and after oxidation using a Mettler model AE240 balance. After oxidation, specimens were examined using scanning electron microscopy with energy dispersive x-ray analysis (SEM/EDXA). Selected samples were analyzed using TEM equipped with EDXA.

Results

Oxidation Behavior of Cast Fe_3Al

In order to fully characterize the effect of an oxide dispersion on the oxidation behavior of Fe_3Al, it is first necessary to illustrate the behavior of the cast material. Above ≈20at%Al, Fe_3Al is a primary alumina-former with no significant transient formation of Fe-rich oxide [8,27]. Like most alumina-formers, there is poor adhesion of the undoped alumina scale. However, the scale formed on Fe_3Al is more highly convoluted than scales observed on MCrAl alloys and β-NiAl, Figure 1a. This results in small pieces of spalled oxide which tend to stick to the substrate, but can be brushed off easily. Reactive element alloy additions of Y and Zr have been shown to improve the scale adhesion [10,11,19], but compared to similar additions to β-NiAl, these additions are not nearly as effective. Figure 2 shows a comparison of total weight gains for Fe_3Al and β-NiAl with and without a Zr addition, during 10 x 100h cycles at 1200°C. While there is an improvement for both alloys with the addition of Zr, the total weight gain on FAL is higher due to scale spallation. Isothermal kinetic data in Figure 3 and Table II indicate that the parabolic growth rate for Fe_3Al + Zr is not significantly different than that for β-NiAl + Zr. However, after just one 100h

cycle, a clear difference in scale adhesion can be observed, Figure 4. At higher magnification, it appears that the substrate deforms and at "peaks" in the substrate, the scale spalls upon cooling. Thus these observations indicate that RE alloy additions are less effective in improving scale adhesion in iron aluminides.

Effects of an Al_2O_3 Dispersion

Several authors have concluded that any stable oxide dispersion, including Al_2O_3, can improve alumina scale adhesion [28-30]. During powder blending, some oxygen uptake is unavoidable and this creates a fine Al_2O_3 dispersion in the consolidated alloy, with a volume fraction proportional to the O content. Several Al_2O_3-dispersed FAS compositions were created in order to study the effect of an Al_2O_3 dispersion, Table I. The most striking effect of the Al_2O_3 dispersion was that it initially produced a flatter, more adherent α-Al_2O_3 scale at 1200°C, Figure 1b. However, on closer examination, it appeared that flattening the scale was the only effect of the Al_2O_3 dispersion. Unlike a typical RE addition, the Al_2O_3 dispersion did not change the scale surface morphology or grain structure, Figures 5 and 6 respectively. The fine surface ridges on cast FAS and Al_2O_3-dispersed FAS are indicative of outward Al transport (Figure 5) as are the whiskers at the gas interface (Figure 6a) [18]. Fine grains at the scale surface are only observed when a RE addition is present, Figure 5c. The cross-sectional grain structure (Figure 6a) is typical of undoped α-Al_2O_3 [18], which grows by the transport of both Al and O along grain boundaries [31-33]. In isothermal experiments at 1200°C, the parabolic rate constant of Al_2O_3-dispersed FAS was

similar to that of cast FAS and an undoped FeCrAl alloy, Table II.

In short-term cyclic testing (20 x 2h) at 1200°C, the Al_2O_3 dispersion was somewhat effective in improving scale adhesion, Figure 7. As mentioned previously, the fine spall on the non-dispersed, extruded FAS tended to stick to the sample. However, during the 20 cycles, the sample began to lose weight. FAS with the highest Al_2O_3 addition, Al_2O_3-1, showed little spallation during the 20 cycles. The flatter scale (Figure 1) was mostly adherent during this short-term testing. FAS with a lower Al_2O_3 addition, Al_2O_3-2, also produced a flat scale after 2h, but spalled readily after a few 2h cycles, Figure 7.

As Figure 8 demonstrates, for longer-term testing (10 x 100h), the Al_2O_3 dispersion was not effective in improving scale adhesion. The almost linear total weight gain indicates that there was nearly complete spallation after each 100h cycle. Examination of the samples by SEM showed scale spallation at the metal-scale interface and the formation of large interfacial voids. Furthermore, when comparing cast and Al_2O_3-dispersed FAS of similar thickness, the Al_2O_3 dispersion significantly shortened the time to breakaway oxidation at 1200°C, Figure 8. Thus, an Al_2O_3 dispersion alone was not effective in improving the oxidation behavior of Fe_3Al.

Reactive Element Oxide Dispersions

The other oxide additions were made at a standard 0.2 cation% level in order to determine the relative effectiveness of the various additions. An initial screening test of 20 x 2h cycles at 1200°C was used in order to assess the performance of the various dopants.

Sample weight change data are shown in Figure 9. As a baseline, Kanthal APM shows almost no spallation during this test with a weight change almost identical to that measured isothermally [18].

As shown in Figure 9, oxide additions of Ce, La and Sc accelerated the oxidation rate and led to FeO formation in the case of the Ce addition [26]. The scale on the La- and Sc- doped alloys was highly convoluted but adherent, e.g. Figure 10. In each case, the addition appeared to cause an acceleration in the oxidation rate (Table II). This detrimental influence has been reported for La_2O_3 additions to β-NiAl [24] and for CeO_2 additions to FeCrAl [34], and is attributed to "over-doping" of the RE addition. In order to test this premise, lower additions of La_2O_3 (0.05%La) and CeO_2 (0.1%) were added to FAS. In short-term testing (Figure 11), this appeared to reduce the negative effects, but, particularly in the case of La, not eliminate them. During longer-term testing (10 x 100h cycles, Figure 12), these lower-doped alloys did not perform well, exhibiting accelerated and breakaway oxidation.

Oxide additions of Y, Nd, Yb, Hf or Zr produced a flat alumina scale after a 2h exposure, similar to that observed with an Al_2O_3 dispersion, Figure 1. However, the scale on each of these alloys spalled to some degree during the 20 x 2h cycles. The similar behavior of these alloys did not sufficiently differentiate the performance of the various dopants. Longer-term testing (Figure 12) showed that Y_2O_3-dispersed FAS performed better than any of the other additions. In isothermal testing, the alloy with a 0.2%Y addition had the lowest parabolic rate (Table II), but the alloys with other dopants did not have significantly higher rates. Rather than a

slower scale growth rate, the lower rate of weight gain of Y_2O_3-dispersed FAS reflects a lower degree of scale spallation relative to the other alloys. The Hf, Nd, Yb and Zr additions did produce some beneficial effect compared to an Al_2O_3 dispersion, for which breakaway oxidation was observed (Figures 3 and 12).

Because of the apparently superior behavior of the Y_2O_3 dispersion, an attempt was made to optimize this addition. However, higher and lower levels of Y in FAS (Table I) did not produce better results than the initial 0.2% addition, Figure 13. It is interesting to note that of the various Y_2O_3 additions, the alloy with a 0.2%Y addition showed slightly more spallation during 20 x 2h cycles (Figure 11 and Reference 24), but the least spallation during 10 x 100h cycles (Figure 13), and the lowest isothermal rate, Table II.

Comparison of the performance of FAS with a 0.2%Y addition to that of cast, Zr-alloyed Fe_3Al indicates that Y_2O_3-dispersed FAS had a lower weight gain during 10 x 100h cycles, Figure 13. This behavior was also observed during 100h cycles at 1300°C, where Y_2O_3-dispersed FAS again showed less spallation than the cast material, Figure 14. Thus, there was some improvement in oxidation behavior of Fe_3Al by the addition of an optimal oxide dispersion. However, in a comparison of Y_2O_3-dispersed FAS to Kanthal APM or β-NiAl+Zr at 1200° and 1300°C (Figures 12-14), the RE dispersion appeared to be less effective in FAS. The higher total weight gain for Y_2O_3-dispersed FAS reflects a greater amount of scale spallation. The ODS FeCrAl and NiAl+Zr showed almost no spallation at either temperature.

Increased Spallation on ODS FAS

The increased degree of spallation on ODS FAS appears to be related to the formation of a large fraction of interfacial voids which grow with time and limit contact between the metal and oxide. Examination of Y_2O_3-dispersed (0.2%Y) FAS after isothermal exposures for 100, 200 and 400h showed an increased degree of spallation with oxidation time. Spallation occurred mainly at the metal-scale interface and not within the scale. Figure 15 shows an increasing fraction of smooth dimpled areas on the exposed metal surface with time. These dimpled regions on the metal surface reflect a loss of contact between the substrate and the α-Al_2O_3 scale, and the formation of an interfacial void. Both the number and size of the voids increased with time.

These voids were also studied on Y_2O_3-dispersed FAS after 2h at 1200°C. before scale spallation occurred, by TEM [35]. Voids were observed along the metal-scale interface, Figure 16. Small (20-50nm) "perturbation" voids were also observed by TEM at the metal-scale interface of ODS FeCrAl alloys [18]. In Y_2O_3-dispersed FAS, the size and frequency of these voids appeared to be greatly increased. If the voids grow with time, the string of voids in Figure 16a might be expected to coalesce to form a much larger void. The alloys with dispersions of Nd, Zr, Yb and Hf were also observed to spall in the same manner and to form a significant volume fraction of interfacial voids.

One possible reason for the increased void formation on FAS is that the high O and N contents (thus larger dispersoid fraction) in the ODS FAS alloys might provide an increase in the number of

nucleation sites compared to commercial ODS FeCrAl (APM, Inco's MA956 and Dour Metal's ODM031, Table I). Using more careful processing techniques, several alloys were produced with lower O and N contents, Table I. However, these ODS alloys instead showed an increased amount of scale spallation, Figure 17. In general, the dopant type and level appeared to be a more critical factor than the O and N contents in determining performance.

Discussion

The results described above and previously reported findings lead to several interesting hypotheses about the evolution of scale and interface morphologies at very high temperatures, and the influence of the substrate on this evolution. The present conclusions regarding the development of scale damage relate to processes that occur isothermally at the oxidation temperature. However, their effects are then manifested in terms of the proclivity for scale spallation during cooling. As such, scale characteristics resulting from cooling stresses must be distinguished from those that develop during high-temperature exposure.

Stress and substrate effects on scale morphology

There are a number of mechanisms by which stresses can develop in the scale and at its interface with the alloy during oxide growth [36]. If scale adherence is maintained, these stresses can be of sufficient magnitude to deform weak substrates and influence the morphology of the growing oxide. Interfacial voids can play an important role in the stress development and the associated

evolution of scale structure. One way this can occur is schematically depicted in Figure 18. Given a typical compressive stress in the plane of the alumina scale, a perturbation caused by a defect, such as an interfacial void (Figure 16) can result in a tensile stress component normal to the metal-scale interface, Figure 18a. With a strong substrate, a void may grow in size without any scale buckling as the oxide layer thickens, Figure 18b. In contrast, as shown in Figure 18c, a weak substrate may accommodate the growth stress by deformation and scale buckling [37]. With additional oxidation, the buckle increases in size and there is further deformation of the substrate, Figure 18d. Variations in scale thickness and cation diffusion distances in the vicinity of the buckle may result in additional local stresses. Thus, buckle formation and growth can be aided by a weak substrate and, with all other factors being equal, at sufficiently high temperature, weaker alloys would be expected to have more convoluted scales upon exposure to an oxidizing environment.

Based on this scale buckling model, any mechanism which results in strengthening of the substrate can affect scale morphology under the appropriate conditions. Oxide dispersions can improve the creep strength of ODS alloys by several orders of magnitude by dislocation pinning (provided the alloy grain size is large) [38]. Therefore, it is not unreasonable to expect that one effect of a dispersed oxide phase on high-temperature oxidation behavior would be to promote a flatter scale by minimizing deformation of the substrate at temperatures where the dispersion-free alloy is quite weak. This mechanism can explain the present observations of a

flatter scale on ODS FAS (whether dispersed with only Al_2O_3 or Al_2O_3 and a RE oxide), Figure 1. The oxide-dispersoid strengthening effect has been observed for FAS with Y_2O_3 [13], but has not been evaluated for Al_2O_3-dispersed FAS because of an inability to significantly increase the grain size. All of the oxidation tests in this study used alloys in the as-extruded, fine ($\approx 1\mu m$) grain condition. Nevertheless, it is possible that some high temperature strengthening of this alloy has also occurred.

Similar strength-scale morphology considerations can be applied to a comparison of the oxidation behavior of cast FAS, FeCrAl, and β-NiAl. Because these alloys typically would not be considered for structural applications at the oxidation temperatures used in the present study, the relevant high temperature strength values are rarely measured. However, a qualitative estimation of the relative strengths is possible from simple visual examination of as-oxidized specimens. These indicate that NiAl is able to support its own weight in the crucible tests at 1200°C and 1300°C, and does not deform as readily as cast FeCrAl or Fe_3Al compositions. A similar comparison indicates that cast FeCrAl is somewhat stronger than cast Fe_3Al. Based on the above model of the effect of substrate strength on scale morphology, these observations explain why the alumina scale on FAS is so highly convoluted while the scale on NiAl after the same exposure (2h at 1200°C) is virtually flat [39]; the stronger NiAl resists deformation. The alumina scale on cast, undoped FeCrAl [18] has fewer convolutions than that observed on Fe_3Al (Figure 1a) consistent with the observation that FeCrAl may be somewhat stronger.

The Effect of an Al_2O_3 dispersion

The RE effect is generally described as an improvement in scale adhesion, a change in the scale growth mechanism (resulting in a reduction in the growth rate), and a modification of the scale microstructure [41]. The results presented here for Al_2O_3-dispersed FAS indicate that this oxide did not produce any of the typical RE effects. The α-Al_2O_3 scale formed at the same rate (Table II) and had the same scale morphology and grain structure (Figures 5 and 6) as a scale formed on an undoped alloy. Thus, there is no reason to believe there was a reduction in growth stresses, yet a flatter scale was formed. Clearly, the present observations with Al_2O_3-dispersed FAS indicate that, while a RE addition might inhibit scale buckling by reducing growth stresses [40], RE doping is not a necessary condition in achieving a flat scale. However, due to the lack of mechanical properties data on these materials, it is not possible at this time to conclude that strengthening the substrate is sufficient to prevent scale buckling. This issue will require more study.

Previously reported beneficial effects for Al_2O_3-dispersed alumina-formers [28,29] may be explained by the strengthening mechanism described above. A flatter scale would remain in better contact with the substrate than a convoluted scale. During longer-term testing, the flat scale fails as a result of the growth of interfacial voids, which limit contact between the scale and substrate. When the void fraction reaches a critical level, the cooling stresses are sufficient to spall the scale. Models have been presented which suggest that indigenous sulfur accelerates the growth of interfacial voids [41-43]. RE additions are able to inhibit this detrimental role

of S, but Al_2O_3-dispersed FAS with no RE addition may not be able to do so. It has been suggested that an Al_2O_3 dispersion could getter S at the dispersoid-matrix interface [44]. If that mechanism was operative, it was not sufficient to improve scale adhesion in this case.

As shown in Figure 8, the Al_2O_3-dispersed FAS exhibited a shorter lifetime than that of the cast FAS (Figure 1). This may be a result of particle coarsening. Large Al_2O_3 particles in the substrate may allow rapid transport of O into the substrate when these particles come into contact with the scale, as has been observed when alumina particles or fibers are introduced into alumina-forming matrices [45,46].

Effects of RE dopants

Based on this study, it appears that when added in the proper amount, RE oxide dispersions in FAS produce all of the RE effects described above (to some degree). Focusing on Y_2O_3-dispersed FAS, scale adhesion was improved (Figures 13 and 14), a microstructure with fine grains at the gas interface (Figure 5c) and columnar grains in cross-section (Figure 6b) was observed, and there was a minor reduction in the scale growth rate (Table II). This scale microstructure and reduction in scale growth rate is similar to that observed for ODS FeCrAl [18]. Based on ^{18}O tracer experiments, the addition of Y_2O_3 or ZrO_2 to FeCrAl inhibits the outward transport of Al, resulting in growth primarily by O inward transport [31-33,39]. The similar growth rate and scale microstructure on Y_2O_3-dispersed FAS is consistent with a similar growth mechanism modification in this case.

For each cation addition, it is expected that there is an optimum dopant level. Therefore, it is not possible at this time to conclude that any of the oxides examined, except Al_2O_3, are ineffective additions. The use of 0.2 cation% appeared to be "over-doping" for additions of La, Ce and Sc. The scale convolutions produced by the La addition (Figure 10) are similar to those observed for scales grown on Y-implanted FeCrAl [47-49]. In both cases, an excessive amount of RE in or near the scale may result in detrimental effects. For example, an excess quantity of segregated cations on scale grain boundaries may allow rapid transport of O. Alternatively, the coarsening of oxide particles in the alloy may allow accelerated oxidation, similar to that suggested for an Al_2O_3 addition. If present in lower concentrations, these dopants may well be effective in improving scale adhesion.

For the case of Y_2O_3 additions, 0.2%Y appeared to be the optimum level. Higher Y_2O_3 contents in ODS FeCrAl have been observed to slightly accelerate oxidation [21]. For the other additions, lower dopant levels may also be more effective for reasons similar to those discussed above. Assuming that the commercial Kanthal APM alloy has an optimized ZrO_2 content of 0.06at% Zr, the 0.2% Zr addition used in this study may not have produced the best effect that could be achieved with Zr-doping. Lower (0.05%) dopant levels of Zr and Hf are currently being investigated that may improve performance (Figure 11).

Although lower RE oxide additions may produce the optimum doping effect on the α-Al_2O_3 scale, the RE addition cannot be reduced below the oxide volume fraction required for strengthening.

Conversely, if the RE oxide content needed for strength improvement reduces the oxidation resistance, then the use of the alloy in high-temperature environments will be problematical. Yttrium may be unique due to its low solubility in these alloys. A fine Y_2O_3-Al_2O_3 oxide dispersion coarsens very slowly and seems to provide the necessary requirements for an optimal RE effect. Elements which are more soluble in the matrix are expected to show faster particle coarsening and diffuse faster into the scale [41].

Based on the results with a Zr alloy addition and RE oxide dispersions, it appears that RE additions to Fe_3Al are not as effective in improving scale adhesion as similar RE additions to FeCrAl and NiAl. (Previous work on ODS FeCrAl and β-NiAl alloys [18,39], has demonstrated that Y and Zr dopants are equally effective in improving alumina scale adhesion.) In Zr-doped NiAl and ZrO_2-dispersed FeCrAl, the RE addition results in a flat adherent scale with minimal interfacial void formation. In the case of cast FAL (0.1%Zr), it appeared that the substrate was deformed and the resulting convoluted scale was subject to spallation, Figure 4a. As suggested earlier, this could be a result of the weak substrate. Although the Zr addition may improve adhesion to some degree by gettering S [50-52] or by decreasing growth stresses [36,40], etc., there may still be sufficient stress at temperature to deform the relatively weak Fe_3Al substrate. The Zr addition would not likely provide much strengthening effect, compared to the cast, undoped FAS, and in fact deformed significantly during crucible oxidation tests at 1200° and 1300°C.

The inability of a Zr alloy addition to prevent scale spallation on Fe_3Al at the temperatures used in this study suggests that there are additional first-order factors, besides sulfur gettering [50-52], which affect scale adhesion. (Zr does have a beneficial effect on scale adhesion at lower oxidation temperatures, where the substrate is stronger and the scale is thinner [10,19]. There is sufficient Zr present to getter the S present in this alloy and yet there is significant scale spallation. However, many of the results on the effect of S were conducted with Ni-base superalloys, which are much stronger at these temperatures. Indigenous S may be less of a factor for a weak substrate.

Smialek et al. [53] also observed scale spallation on Fe-40%Al with Hf and Zr alloy additions. They concluded that the inability of these RE additions to prevent scale spallation was related to a larger difference in the coefficient of thermal expansion between α-Al_2O_3 and iron aluminides than other alumina-formers. The present results suggest that, rather than excessive damage during cooling, scale spallation on RE-alloyed iron aluminides was a result of scale buckling which occurred isothermally. Void formation might have been suppressed by the Zr addition, but scale buckling appeared to lead to cracking and spallation (shown schematically in Figure 18c) during cooling.

In the case of Y_2O_3-dispersed FAS, the substrate may be sufficiently strengthened that there is some improvement over a Zr addition to the cast alloy. The deformation mechanism may no longer lead to a spallation-prone scale morphology. However, a second mechanism, the growth of interfacial voids, appeared to limit

performance relative to ODS FeCrAl. The excessive formation of interfacial voids may be similar to that observed on β-NiAl [54]. Due to the diffusion characteristics of the ordered Fe_3Al matrix (unlike a FeCrAl alloy), these materials may be inherently more susceptible to Kirkendall-type voids at the oxidation front. This idea and others are currently being investigated.

The higher spallation rate of ODS FAS means an increased Al consumption rate. This reduces the potential lifetime benefits of the high Al content of Fe_3Al [6,11]. Thus, attempts to improve scale adhesion are a critical step in the development of these materials.

Conclusions

1. At 1200° and 1300°C, incorporation of a reactive element in Fe_3Al as an oxide dispersion is more effective in improving scale adhesion than a comparable elemental addition. It is proposed that this is due to strengthening of the substrate.
2. Al_2O_3 dispersions also strengthen the Fe_3Al substrate and reduce the amount of scale buckling. However, the scale grain structure is not modified and no long-term benefit to oxidation resistance is achieved.
3. Currently, the best ODS Fe_3Al spalls more readily than commercial ODS FeCrAl alloys. This is attributed to more rapid interfacial void nucleation and growth in ODS Fe_3Al.
4. Comparison of the oxidation behavior of Fe_3Al with various oxide dispersions at 1200°C indicates that no addition was superior to Y_2O_3 in conferring a beneficial effect.

Acknowledgments

The authors would like to thank J. R. DiStefano, J. H. DeVan, D. F. Wilson and K. B. Alexander at ORNL for their comments on the manuscript; R. K. Williams for assistance with preparing the oxide powders; K. B. Alexander and P. J. Maziasz at ORNL and R. N. Wright at INEL for TEM contributions; and K. S. Blakely, L. D. Chitwood, M. Howell, J. Weaver and J. W. Jones for assistance with the experimental work. This research was sponsored by the U.S. Department of Energy, Fossil Energy AR&TD Materials Program under contract DE-AC05-96OR22464 with Lockheed Martin Energy Research Corporation. BAP is supported by the U. S. Department of Energy Distinguished Postdoctoral Research Program administered by the Oak Ridge Institute for Science and Education.

References

1. *F. Starr, A. R. White, B. Kazimierzak* in: Materials for Advanced Power Engineering 1994, Eds. D. Coutsouradis, et al.; Kluwer Academic Publishers, Dordrecht, 1994 p. 1393.
2. *W. J. Quadakkers, K. Bongartz, F. Schubert, H. Schuster* in: Materials for Advanced Power Engineering 1994, Eds. D. Coutsouradis, et al.; Kluwer Academic Publishers, Dordrecht, 1994 p. 1533.
3. *W. J. Quadakkers, M. J. Bennett*: Mat. High Temp. 10 (1994) 126.
4. *W. J. Quadakkers, K. Bongartz*: Werkst. Korros. 45 (1994) 232
5. *M. J. Bennett, R. Perkins, J. B. Price, N. Starr* in: Materials for Advanced Power Engineering 1994, Eds. D. Coutsouradis, et al.; Kluwer Academic Publishers, Dordrecht, 1994 p. 1553.
6. *I. G. Wright, B. A. Pint, C. S. Simpson, P. F. Tortorelli*: "High Temperature Oxidation Life Characteristics of ODS Fe_3Al," Materials Science Forum, in press (1996).

7. *C. Sykes J. W. Bampfylde*: J. Iron and Steel Inst. 130, 389 (1934).
8. *P. Tomaszewicz, G. R. Wallwork*: Rev. High Temp. Mat. 4, 75 (1978).
9. *C. G. McKamey, J. H. DeVan, P. F. Tortorelli, V. K. Sikka*: J. Mater. Res. 6, 1779 (1991).
10. *P. F. Tortorelli, J. H. DeVan* in: Processing, Properties, and Applications of Iron Aluminides, Eds. J. H. Schneibel, M. A. Crimp; TMS, Warrendale, PA, 1994, p.257.
11. *J. H. DeVan, P. F. Tortorelli, M. J. Bennett* in: Proc. Eighth Annual Conf. Fossil Energy Materials, CONF-9405143, Eds. N. C. Cole, R. R. Judkins; U. S. Department of Energy, Washington, D.C., 1994, p.316.
12. *C. G. McKamey, P. J. Maziasz, J. W. Jones*: J. Mater. Res. 7 (1992) 2089.
13. *I. G. Wright, C. G. McKamey, B. A. Pint* in: Proc. Ninth Annual Conf. Fossil Energy Materials, CONF-9505204, Eds. N. C. Cole, R. R. Judkins; U. S. Department of Energy, Washington, D.C., 1995, p.355.
14. *P. F. Tortorelli, J. H. DeVan, G. M. Goodwin, M. Howell* in: Elevated Temperature Coatings: Science and Technology I, Eds. N. B. Dahorte, J. M. Hampikian, J. J. Stiglich; TMS, Warrendale, PA, 1995, p.203.
15. *P. F. Tortorelli, I. G. Wright, G. M. Goodwin, M. Howell* in: High Temperature Coatings II, Eds. N. B. Dahorte, J. M. Hampikian; TMS, Warrendale, PA, 1996, in press.
16. *T. Raghavan, L. Steeds, R. Petkovic-Luton*: Met. Trans., 13A (1982) 953.
17. *I. S. Polkin, E. V. Ivanova, B. P. Matyhin* in: Structural Applications of Mechanical Alloying, Eds. F. H. Froes, J. J. deBarbadillo, ASM International, Materials Park, OH, 1990 p.131.
18. *B. A. Pint, A. J. Garratt-Reed, L. W. Hobbs*: Mat. High Temp. 13 (1995) 3.
19. *P. F. Tortorelli, J. H. DeVan, U. K. Abdali* in: Corrosion 93, NACE, Houston, TX, 1993, p.258/1-9.
20. *M. J. Bennett, M. R. Houlton* in: High Temperature Materials for Power Engineering, Eds. E. Bachelet, et al.; Kluwer Academic Publishers, Amsterdam, 1990, p. 227.
21. *W. J. Quadakkers, K. Schmidt, H. Grubmeier, E. Wallura*: Mat. High Temp. 10 (1992) 23.
22. *H. T. Michels*: Met. Trans. 9A (1978) 873.
23. *K. L. Luthra, E. L. Hall*: Oxid. Met. 26 (1986) 385.

24. *B. A. Pint, L. W. Hobbs* in: High Temperature Ordered Intermetallics VI, Eds. J. Horton, S. Hanada, I. Baker, R. D. Noebe, D. Schwartz; Symp. Proc. v.364, Materials Research Society, Pittsburgh, PA, 1995, p.987.
25. *B. A. Pint*: "The Oxidation Behavior of Oxide-Dispersed β-NiAl: I. Short-Term Cyclic Data and Scale Morphology," submitted to Oxidation of Metals.
26. *B. A. Pint, K. B. Alexander, P. F. Tortorelli* in: High Temperature Ordered Intermetallics VI, Eds. J. Horton, S. Hanada, I. Baker, R. D. Noebe, D. Schwartz; Symp. Proc. v.364, Materials Research Society, Pittsburgh, PA, 1995, p.1315.
27. *J. H. DeVan, P. F. Tortorelli*: Corr. Sci., 35 (1993) 1065.
28. *J. K. Tien, F. S. Pettit*: Met. Trans. 3 (1972) 1587.
29. *L. M. Kingsley, J. Stringer*: Oxid. Met. 32 (1989) 371.
30. *D. P. Whittle, J. Stringer*: Phil. Trans. Royal Soc. London, Serial A 295 (1980) 309.
31. *W. J. Quadakkers, H. Holzbrecher, K. G. Briefs, H. Beske*: Oxid. Met. 32 (1989) 67.
32. *B. A. Pint, J. R. Martin, L. W. Hobbs*: Oxid. Met. 39 (1993) 167.
33. *D. Clemens, K. Bongartz, W. Speier, R. J. Hussey, W. J. Quadakkers*: Fresenius' J. Anal. Chem. 346 (1993) 318.
34. *B. A. Pint*: "Study of the Reactive Element Effect in ODS Iron-Base Alumina-Formers," Materials Science Forum, in press (1996).
35. *K. B. Alexander, B. A. Pint*: Oak Ridge National Laboratory, unpublished research 1996.
36. *F. H. Stott, A. Atkinson*: Mat. High Temp. 12 (1994) 195.
37. *H. E. Evans*: Int. Mat. Rev. 40 (1995) 1.
38. *F. H. Froes, J. J. deBarbadillo* in: Structural Applications of Mechanical Alloying, Eds. F. H. Froes, J. J. deBarbadillo, ASM International, Materials Park, OH, 1990 p.131.
39. *B. A. Pint*: Ph.D. Thesis, Massachusetts Institute of Technology, Cambridge, MA, 1992.
40. *F. A. Golightly, F. H. Stott, G. C. Wood*: Oxid. Met. 10 (1976) 163.
41. *B. A. Pint*: Oxid. Met. 45 (1996) 1.
42. *H. J. Grabke, D. Weimer, H. Viefhaus*: App. Surf. Sci. 47 (1991) 243.
43. *B. A. Pint*: "On the Formation of Interfacial and Internal Voids in α-Al_2O_3 Scales" submitted to Oxidation of Metals.
44. *D. G. Lees*: Oxid. Met. 27 (1987) 75.
45. *J. Doychak, J. A. Nesbitt, R. D. Noebe, R. R. Bowman*: Oxid. Met. 38 (1992) 45

46. *P. F. Tortorelli, J. H. DeVan, C. G. McKamey, M. Howell*: Ceram Trans. 19 (1991) 961.
47. *J. G. Smeggil, A. J. Shuskus*: J. Vac. Sci. Tech. A 4 (1986) 2577.
48. *J. Jedlinski, G. Borchardt, S. Mrowec*: Werkst. Korros. 41 (1990) 701.
49. *W. J. Quadakkers, J. Jedlinski, K. Schmidt, M. Krasovec, G. Borchardt, H. Nickel*: App. Surf. Sci., 47, 261 (1991).
50. *A. W. Funkenbush, J. G. Smeggil, N. S. Bornstein*: Met. Trans. 16A (1985) 1164
51. *J. L. Smialek*: Met. Trans. 22A (1991) 739
52. *D. R. Sigler*: Oxid. Met. 32 (1989) 337
53. *J. L. Smialek, J. Doychak, D. J. Gaydosh*: Oxid. Met. 34 (1990) 259.
54. *M. W. Brumm, H. J. Grabke*: Corr. Sci. 34 (1993) 547.

List of Figures

Figure 1. SEM secondary electron images of the scale surface after 2h at 1200°C in O_2 (a) unmilled, extruded Fe-28Al-2Cr powder, (b) milled, extruded powder which contains an Al_2O_3 dispersion and (c) milled, extruded powder which contains a Y_2O_3 dispersion. The addition of an oxide dispersion flattens the α-Al_2O_3 scale on Fe_3Al.

Figure 2. Total weight change (sample + spalled oxide) during 100h cycles at 1200°C for β-NiAl and Fe_3Al, with and without a Zr alloy addition. β-NiAl + Zr shows almost no scale spallation during 10 cycles, while the other alloys show significant spallation. The Zr addition is not nearly as effective in improving scale adhesion in Fe_3Al.

Figure 3. Parabolic plot of weight gain versus square root of time for Zr-doped β-NiAl and Fe_3Al alloys at 1200°C in 1 atm O_2.

Figure 4. SEM secondary electron plan views of the α-Al_2O_3 scale formed after oxidation in 1 atm O_2 for 100h at 1200°C on (a) Fe-28Al-5Cr-0.1Zr (FAL) and (b) Ni-50Al-0.04at%Zr. Some scale spallation is observed on FAL but not on Zr-doped β-NiAl.

Figure 5. SEM secondary electron images of the alumina scale surface after 2h at 1200°C in O_2 (a) unmilled, extruded Fe-28Al-2Cr powder, (b) milled, extruded powder which contains an Al_2O_3 dispersion and (c) milled, extruded powder which contains a Y_2O_3 dispersion. At high magnification, there is little effect of the Al_2O_3 dispersion on the scale morphology compared to a Y_2O_3 dispersion.

Figure 6. SEM secondary electron images of fracture sections of the α-Al_2O_3 scale formed after oxidation in 1atm O_2 for 100h at 1200°C on Fe-28Al-2Cr (FAS) dispersed with (a) Al_2O_3 and (b) Y_2O_3. The grains in (a) are somewhat elongated but do not have the same columnar structure as with Y_2O_3-doping. The Y_2O_3 addition also eliminates the whisker formation shown in (a).

Figure 7. Sample weight change of several alloys cycled from room temperature to 1200°C with a cycle time at temperature of 2h. ZrO_2-dispersed FeCrAl exhibits virtually no spallation during this test.

Figure 8. Total weight change (sample + spalled oxide) during 100h cycles at 1200°C for Kanthal APM and undoped Fe_3Al with various O contents. In long-term testing, ZrO_2-dispersed FeCrAl showed excellent scale adhesion but Al_2O_3 dispersions did not improve scale adhesion and instead shortened the time to breakaway compared to a cast alloy. The extruded FAS appeared to "slump" and rapidly oxidize.

Figure 9. Sample weight change of Fe-28Al-2Cr (FAS) with various cation oxide dispersions (0.2 at%) cycled from room temperature to 1200°C with a cycle time at temperature of 2h. None of the alloys perform as well as ZrO_2-dispersed FeCrAl.

Figure 10. SEM secondary electron image of the alumina scale surface formed on La_2O_3-dispersed (0.2%La) FAS after 50h at 1200°C in O_2. The highly convoluted scale results in an accelerated oxidation rate.

Figure 11. Sample weight change of Fe-28Al-2Cr (FAS) with various cation oxide dispersions after 2h cycles at 1200°C. By reducing the initial 0.2 cation% dopant level, improved performance was observed for additions of CeO_2 and La_2O_3. Similar improvements may be possible for reduced levels of HfO_2 and ZrO_2. Various Y_2O_3 contents showed little change in performance.

Figure 12. Total weight change (sample + spalled oxide) during 100h cycles at 1200°C for Kanthal APM and various oxide dispersions in FAS. La, Ce and Sc additions resulted in accelerated oxidation. None of the other additions performed as well in FAS as Y_2O_3.

Figure 13. Total weight change (sample + spalled oxide) during 100h cycles at 1200°C for cast FAL (0.1Zr), β-NiAl+Zr and various oxide dispersions to FAS. A 0.2cation%Y addition to FAS resulted in the best Fe_3Al performance. Different Y contents did not show improved performance.

Figure 14. Total weight change (sample + spalled oxide) during 100h cycles at 1300°C for several materials. As at 1200°C, the ODS Fe_3Al outperformed cast Fe_3Al + Zr but showed more scale spallation than ODS FeCrAl or β-NiAl+Zr.

Figure 15. SEM secondary electron images of the Y_2O_3-dispersed FAS metal surface after oxidation at 1200°C in O_2 for (a) 100h (b) 200h

and (c) 400h. The void fraction (smooth areas) increased with oxidation time.

Figure 16. TEM bright field image of the metal-scale interface of Y_2O_3-dispersed Fe-28Al-2Cr after 2h at 1200°C in O_2. The arrows mark interfacial voids [35].

Figure 17. Sample weight change of Fe-28Al-2Cr (FAS) with various cation oxide dispersions cycled from room temperature to 1200°C with a cycle time at temperature of 2h. A larger amount of spallation was observed when the O content was reduced.

Figure 18. A scale buckling model (a) with compressive, in-plane growth stresses in the oxide scale, a defect such as an interfacial void results in a normal tensile stress; (b) with a strong substrate, the void may continue to grow but no deformation occurs; (c) with a weak substrate, the metal is deformed by the tensile stress and the scale begins to buckle (dashed line marks the original metal interface), the buckle may crack and spall during cooling; (d) the buckle can continue to grow, leading to increased growth stresses due to the geometry and the range of diffusion distances for Al.

Table I. Chemical analysis of the as-extruded alloys. Concentrations (in atomic percent) were determined by inductively coupled plasma analysis. Sulfur, oxygen and nitrogen contents were determined by combustion analysis.

FAS:	dopant (at%)	Al (at%)	Cr (at%)	O (at%)	N (at%)	S (ppm)	Si (at%)	Ti (at%)
Cast	<0.01 Y	28.40	2.00	0.01	0.001	29	<0.01	<0.01
Extruded	<0.01 Y	24.81	2.04	0.10	0.24	48	n.d.	0.08
Al_2O_3-1	<0.01 Y	25.91	1.94	6.33	2.89	61	0.13	0.07
Al_2O_3-2	<0.01 Y	27.34	2.21	2.34	0.67	62	0.20	0.08
Al_2O_3-3	<0.01 Y	29.84	2.81	1.32	0.10	24	0.32	<0.01
Ce	0.19	26.60	1.98	4.88	3.24	53	0.19	0.08
Ce	0.10	28.88	2.63	3.31	0.40	24	0.60	<0.01
Hf	0.18	29.77	2.21	1.63	0.13	24	0.71	<0.01
La	0.16	26.49	1.98	4.23	2.37	62	0.10	0.06
La	0.04	25.68	1.89	6.57	3.20	60	0.11	0.07
Nd	0.17	27.39	2.13	2.39	0.65	60	0.05	0.08
Sc	0.19	29.16	2.76	1.90	0.19	23	0.63	<0.01
Y	0.05	26.17	2.13	5.06	0.42	54	0.18	0.07
Y	0.09	25.75	2.19	5.33	0.24	51	n.d.	0.07
Y-low O	0.17	29.22	2.74	2.03	0.30	21	0.66	<0.01
Y	0.19	26.92	2.39	3.03	0.11	49	n.d.	0.07
Y	0.28	26.84	2.33	3.35	0.16	54	n.d.	0.08
Y	0.46	26.60	2.26	3.90	0.23	50	n.d.	0.08
Yb	0.29	27.04	2.06	3.67	1.27	63	0.10	0.07
Zr	0.17	27.21	2.16	2.73	0.32	70	0.05	0.07
APM†	0.06 Zr	10.65	20.37	0.17	n.d.	10	0.43	0.03
NiAl	<0.01 Zr	50.23	<0.01	n.d.	n.d.	20	<0.01	n.d.
NiAl	0.04 Zr	49.65	<0.01	n.d.	0.02	35	n.d.	<0.01
FAL	0.10 Zr	27.23	5.14	0.04	0.01	53	<0.01	<0.01
MA956†	0.30 Y	8.40	19.39	0.66	n.d.	110	n.d.	0.39
ODM031	0.24 Y	6.65	13.29	1.16	0.08	71	0.09	0.67

† from reference 18.

Table II. Parabolic oxidation rate constants at 1200°C for isothermal exposures in dry, flowing O_2 (except where noted).

Alloy	Rate Constant (g^2/cm^4s) 1200°C	# of tests
Extruded FAS	1.3×10^{-11} [a]	1
FAS + Al_2O_3	$1.1\text{-}1.5 \times 10^{-11}$	2
FAS + Al_2O_3	$8.8\text{-}9.6 \times 10^{-12}$	3
FAS + 0.05Y	5.6×10^{-12}	1
FAS + 0.1Y	7.4×10^{-12}	1
FAS + 0.2Y	$2.5\text{-}3.5 \times 10^{-12}$	3
FAS + 0.3Y	3.9×10^{-12}	1
FAS + 0.5Y	$5.7\text{-}6.0 \times 10^{-12}$	2
FAS + 0.2Ce	breakaway	1
FAS + 0.1Ce	6.9×10^{-12}	1
FAS + 0.2Hf	1.1×10^{-11}	1
FAS + 0.2La	b	1
FAS + 0.2Nd	5.0×10^{-12}	1
FAS + 0.2Sc	1.3×10^{-11}	1
FAS + 0.2Yb	5.1×10^{-12}	1
FAS + 0.2Zr	5.3×10^{-12}	1
FAL (Fe_3Al + Zr)	$6.0\text{-}7.4 \times 10^{-12}$	2
β-NiAl + Zr	$2.7\text{-}4.5 \times 10^{-12}$	5
Undoped FeCrAl	1.8×10^{-11} [c]	2
FeCrAl + ZrO_2	$3\text{-}4 \times 10^{-12}$ [c]	3

[a] from reference 26, experiments performed in dry, flowing air

[b] accelerated oxidation rate, not parabolic

[c] from reference 18

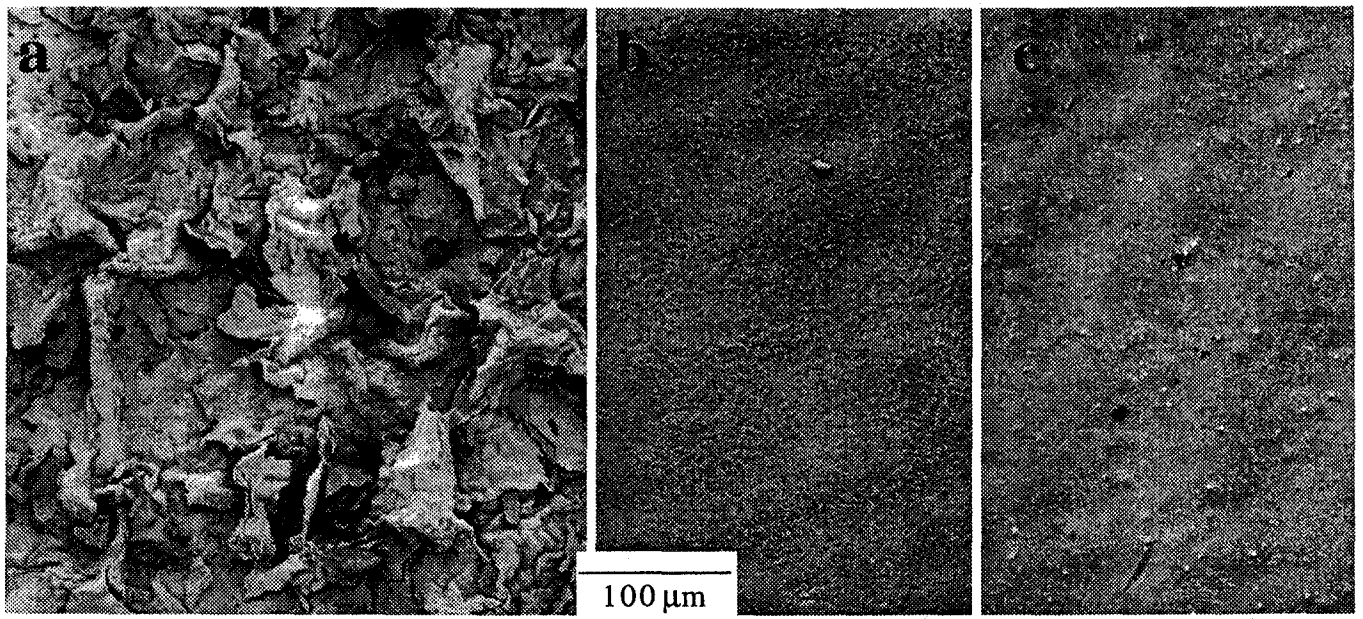

Figure 1. SEM secondary electron images of the scale surface after 2h at 1200°C in O_2 (a) unmilled, extruded Fe-28Al-2Cr powder, (b) milled, extruded powder which contains an Al_2O_3 dispersion and (c) milled, extruded powder which contains a Y_2O_3 dispersion. The addition of an oxide dispersion flattens the α-Al_2O_3 scale on Fe_3Al.

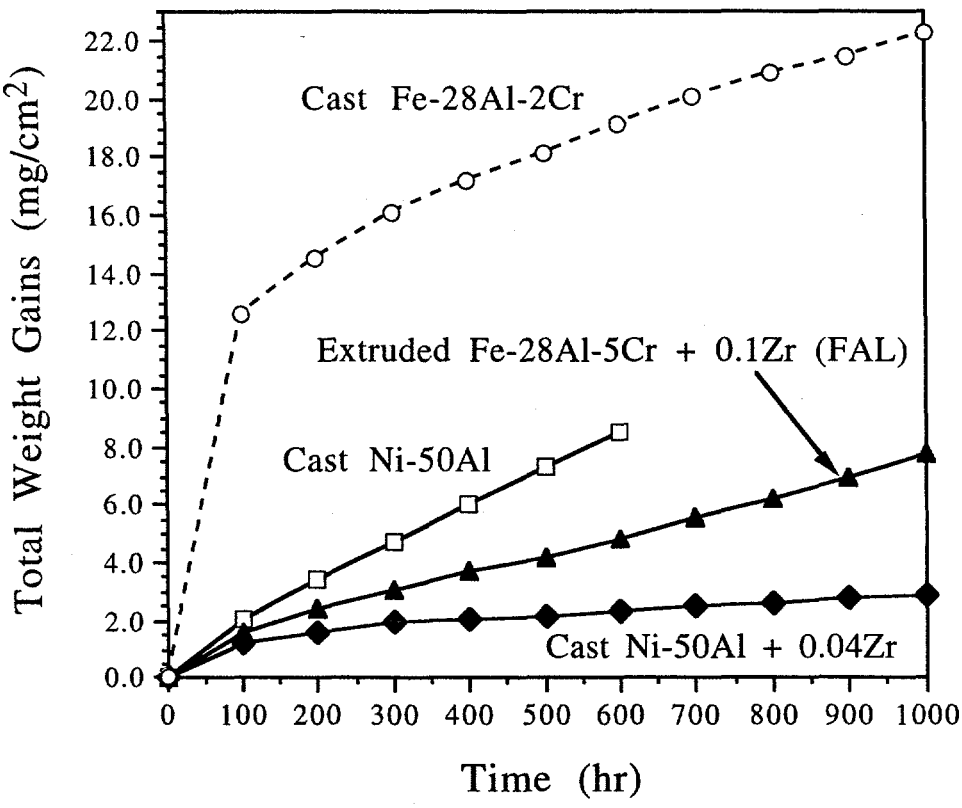

Figure 2. Total weight change (sample + spalled oxide) during 100h cycles at 1200°C for β-NiAl and Fe_3Al, with and without a Zr alloy addition. β-NiAl + Zr shows almost no scale spallation during 10 cycles, while the other alloys show significant spallation. The Zr addition is not nearly as effective in improving scale adhesion in Fe_3Al.

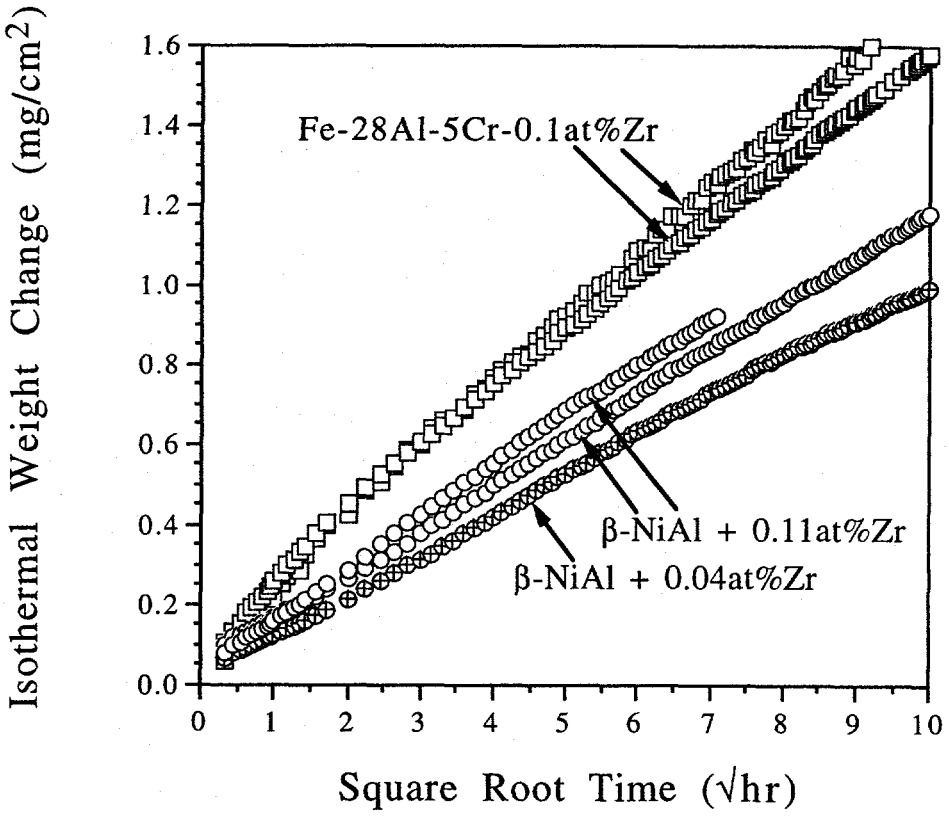

Figure 3. Parabolic plot of weight gain versus square root of time for Zr-doped β-NiAl and Fe_3Al alloys at 1200°C in 1 atm O_2.

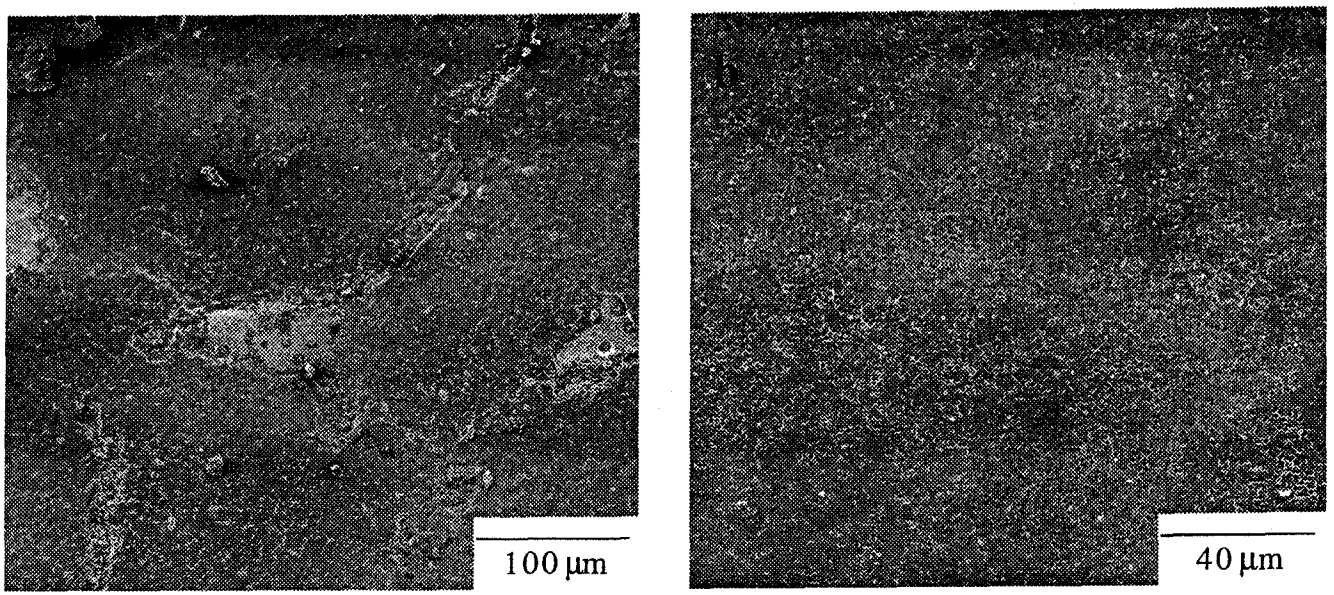

Figure 4. SEM secondary electron plan views of the α-Al_2O_3 scale formed after oxidation in 1 atm O_2 for 100h at 1200°C on (a) Fe-28Al-5Cr-0.1Zr (FAL) and (b) Ni-50Al-0.04at%Zr. Some scale spallation is observed on FAL but not on Zr-doped β-NiAl.

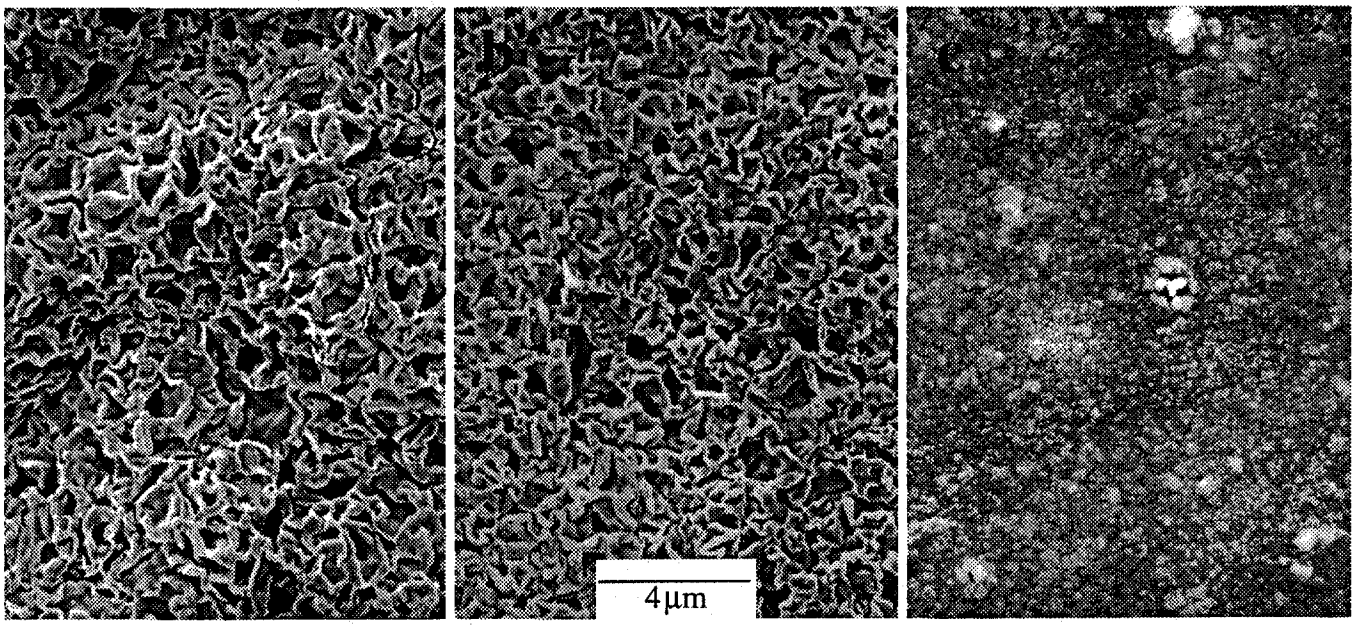

Figure 5. SEM secondary electron images of the alumina scale surface after 2h at 1200°C in O_2 (a) unmilled, extruded Fe-28Al-2Cr powder, (b) milled, extruded powder which contains an Al_2O_3 dispersion and (c) milled, extruded powder which contains a Y_2O_3 dispersion. At high magnification, there is little effect of the Al_2O_3 dispersion on the scale morphology, compared to a Y_2O_3 dispersion.

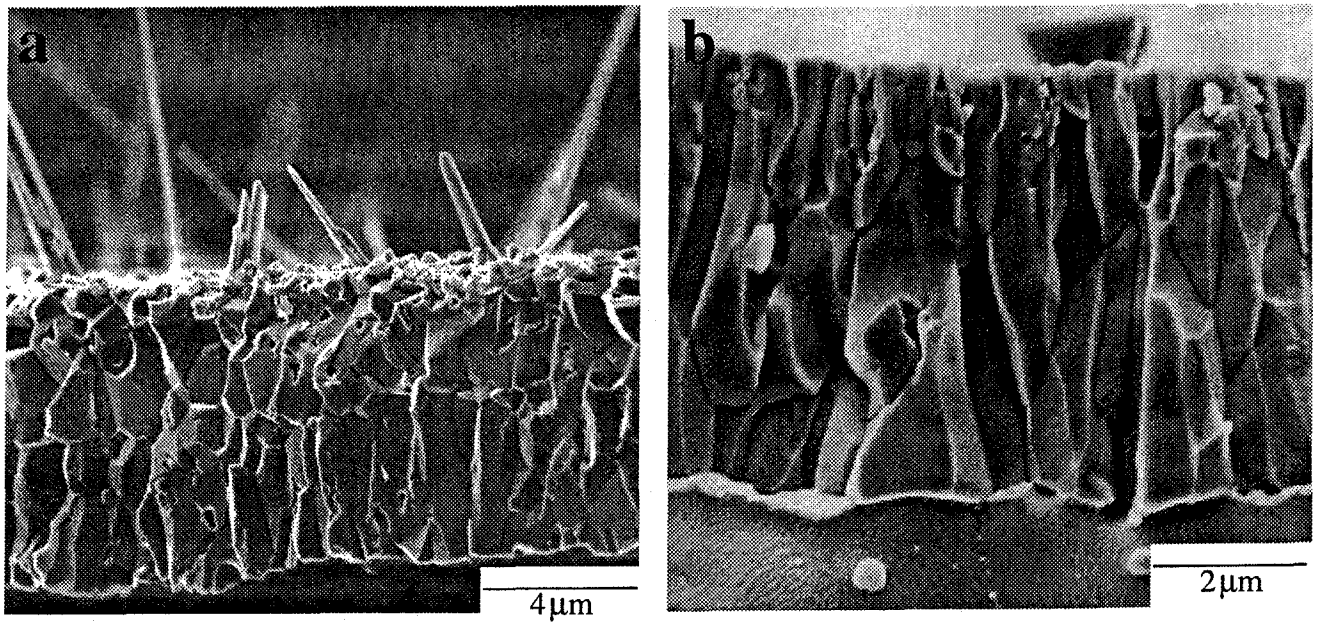

Figure 6. SEM secondary electron images of fracture sections of the α-Al_2O_3 scale formed after oxidation in 1atm O_2 for 100h at 1200°C on Fe-28Al-2Cr (FAS) dispersed with (a) Al_2O_3 and (b) Y_2O_3. The grains in (a) are somewhat elongated but do not have the same columnar structure as with Y_2O_3-doping. The Y_2O_3 addition also eliminates the whisker formation shown in (a).

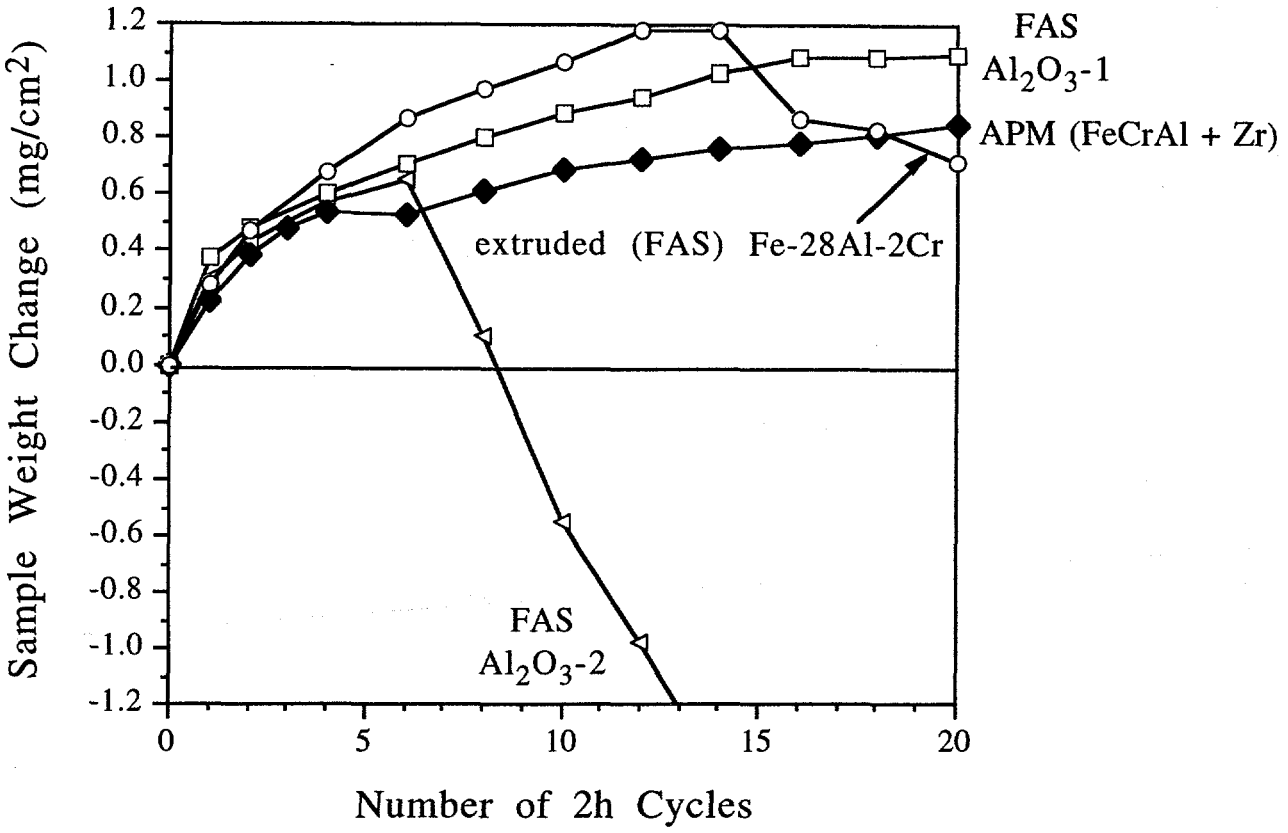

Figure 7. Sample weight change of several alloys cycled from room temperature to 1200°C with a cycle time at temperature of 2h. ZrO_2-dispersed FeCrAl exhibits virtually no spallation during this test.

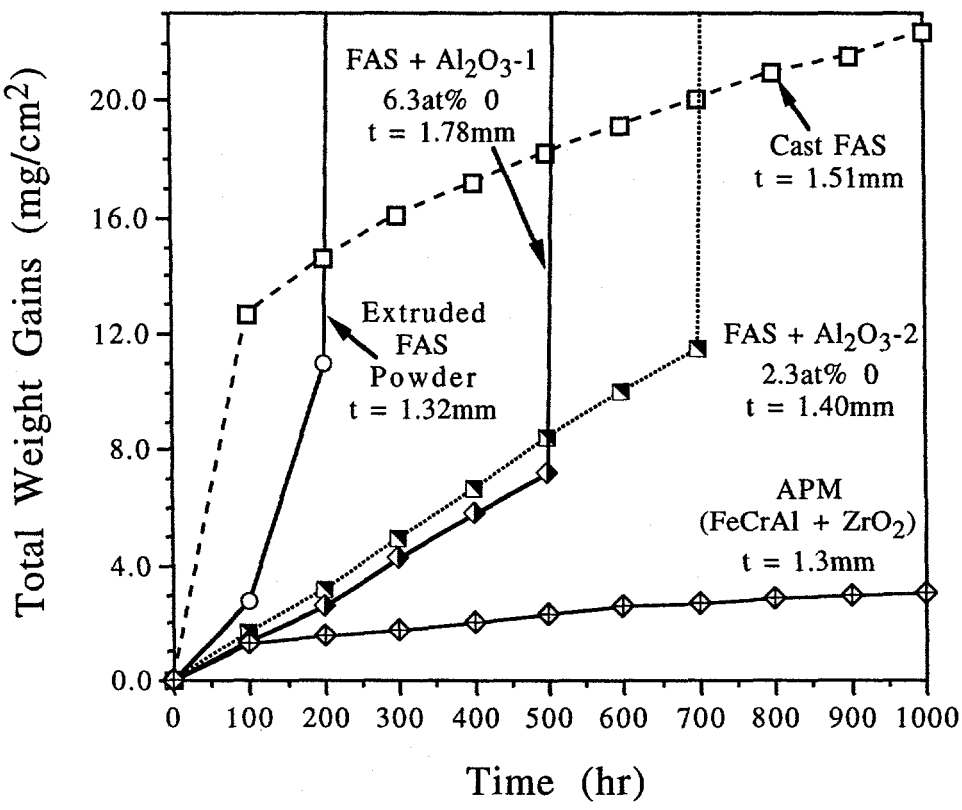

Figure 8. Total weight change (sample + spalled oxide) during 100h cycles at 1200°C for Kanthal APM and undoped Fe_3Al with various O contents. In long-term testing, ZrO_2-dispersed FeCrAl showed excellent scale adhesion but Al_2O_3 dispersions did not improve scale adhesion and instead shortened the time to breakaway compared to a cast alloy. The extruded FAS appeared to "slump" and rapidly oxidize.

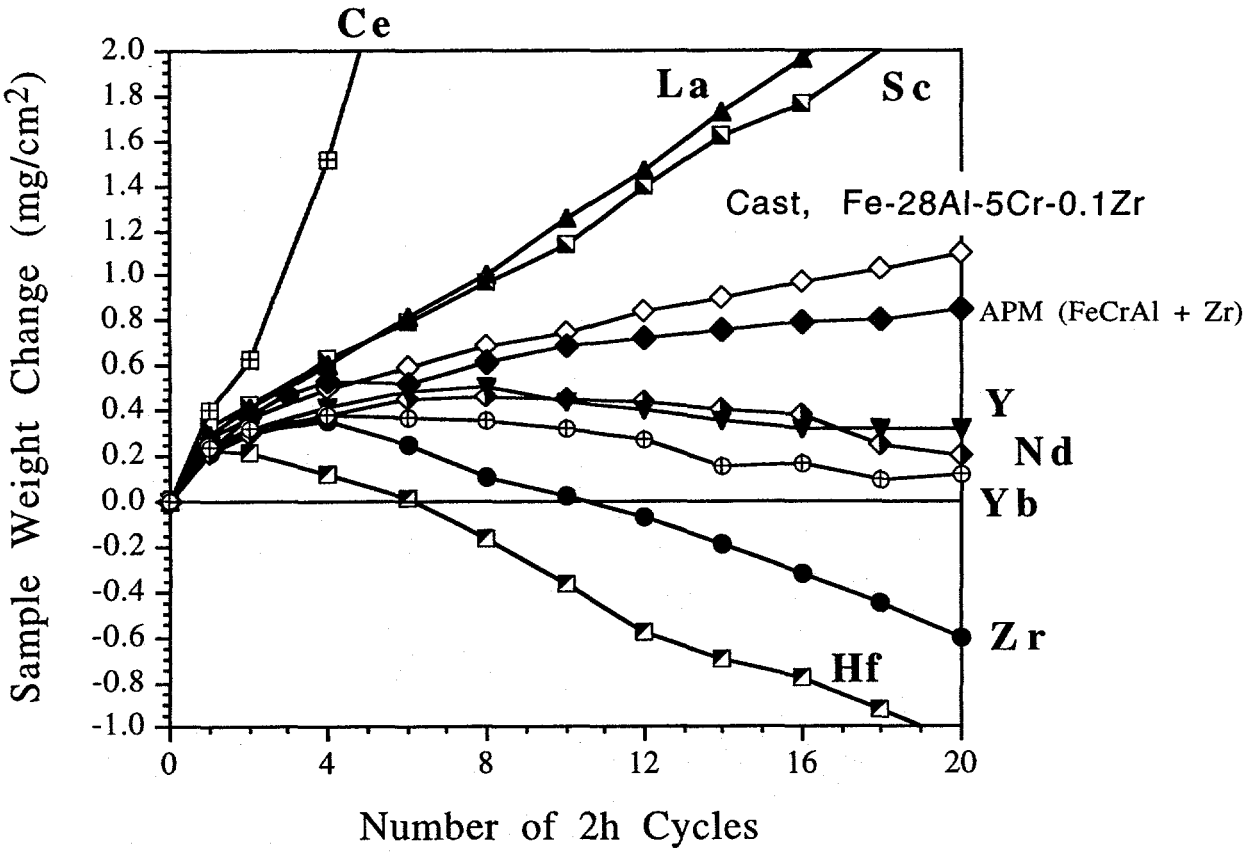

Figure 9. Sample weight change of Fe-28Al-2Cr (FAS) with various cation oxide dispersions (0.2 at%) cycled from room temperature to 1200°C with a cycle time at temperature of 2h. None of the alloys perform as well as ZrO_2-dispersed FeCrAl.

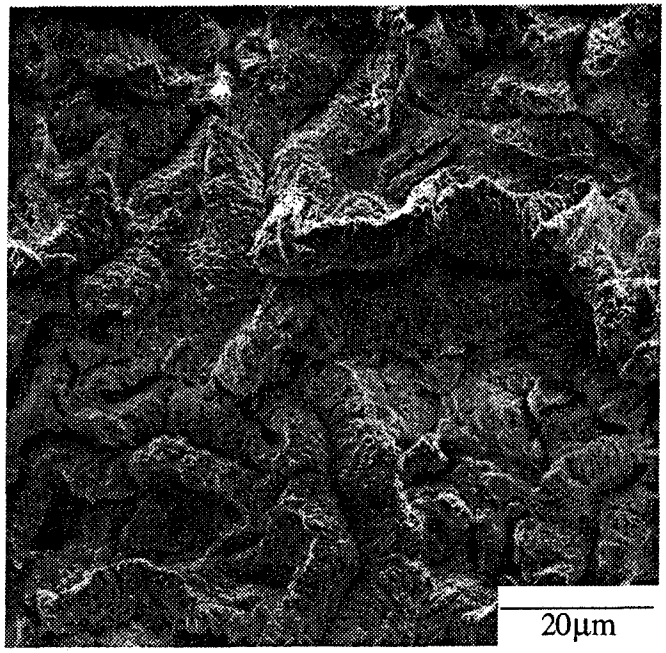

Figure 10. SEM secondary electron image of the alumina scale surface formed on La_2O_3-dispersed (0.2%La) FAS after 50h at 1200°C in O_2. The highly convoluted scale results in an accelerated oxidation rate.

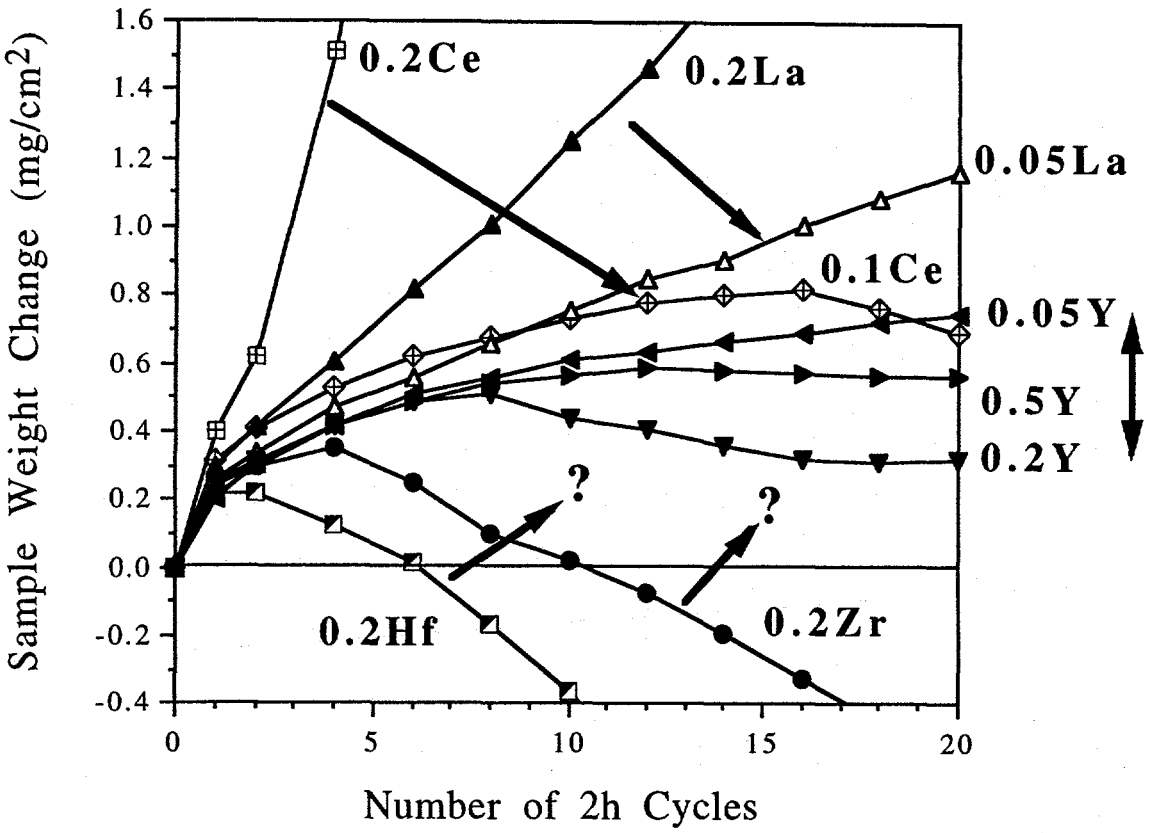

Figure 11. Sample weight change of Fe-28Al-2Cr (FAS) with various cation oxide dispersions after 2h cycles at 1200°C. By reducing the initial 0.2 cation% dopant level, improved performance was observed for additions of CeO_2 and La_2O_3. Similar improvements may be possible for reduced levels of HfO_2 and ZrO_2. Various Y_2O_3 contents showed little change in performance.

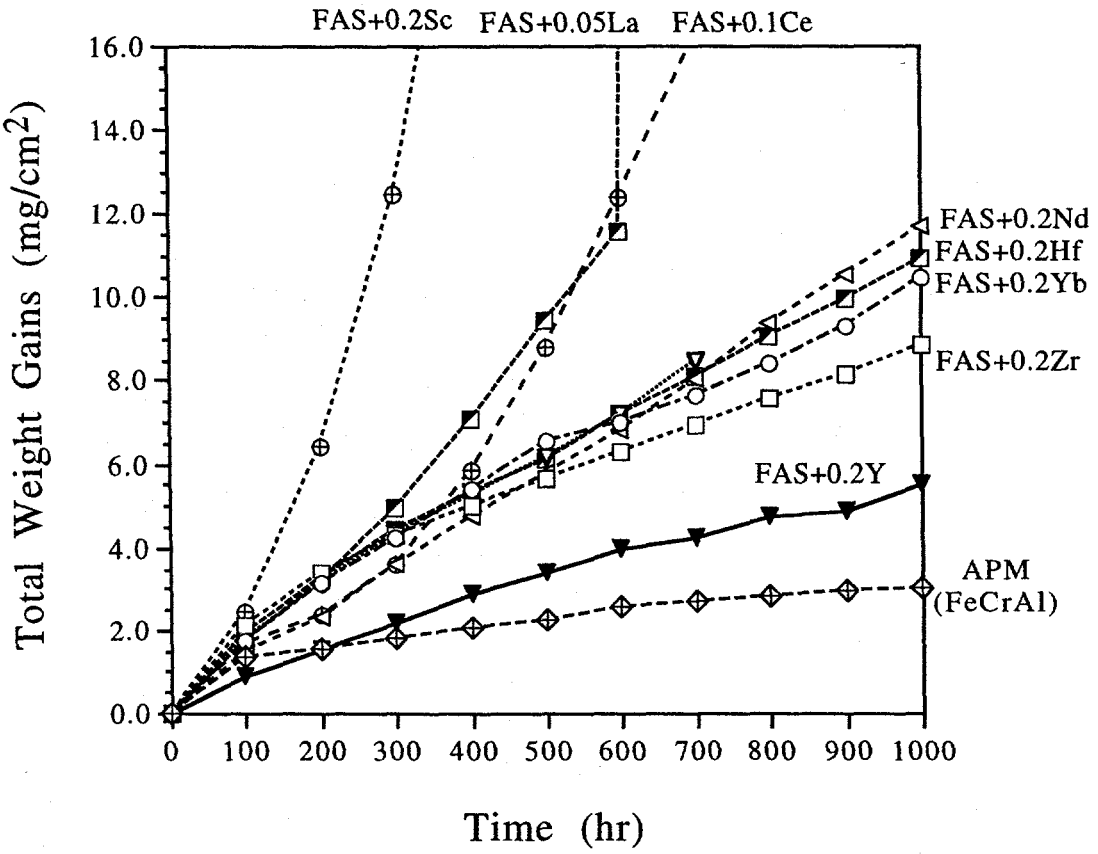

Figure 12. Total weight change (sample + spalled oxide) during 100h cycles at 1200°C for Kanthal APM and various oxide dispersions in FAS. La, Ce and Sc additions resulted in accelerated oxidation. None of the other additions performed as well in FAS as Y_2O_3.

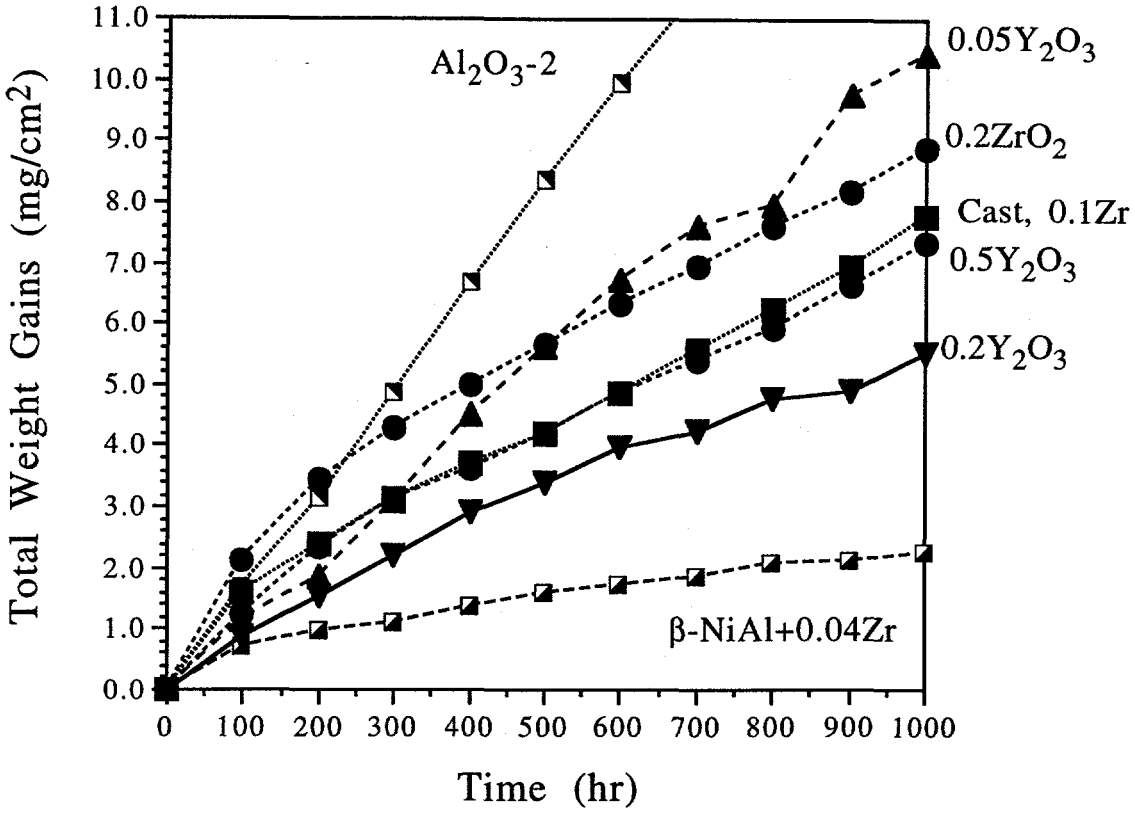

Figure 13. Total weight change (sample + spalled oxide) during 100h cycles at 1200°C for cast FAL (0.1Zr), β-NiAl+Zr and various oxide dispersions to FAS. A 0.2cation%Y addition to FAS resulted in the best Fe_3Al performance. Different Y contents did not show improved performance.

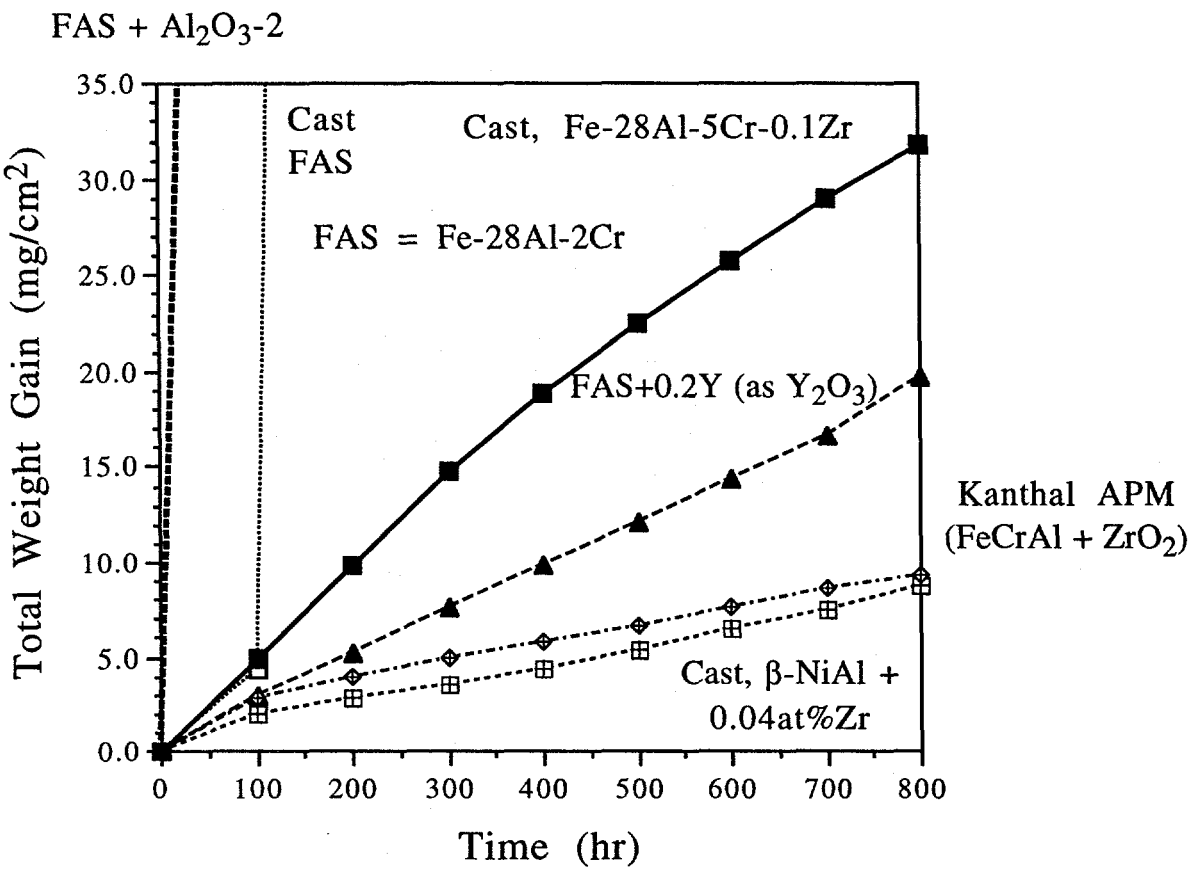

Figure 14. Total weight change (sample + spalled oxide) during 100h cycles at 1300°C for several materials. As at 1200°C, the ODS Fe_3Al outperformed cast Fe_3Al + Zr but showed more scale spallation than ODS FeCrAl or β-NiAl+Zr.

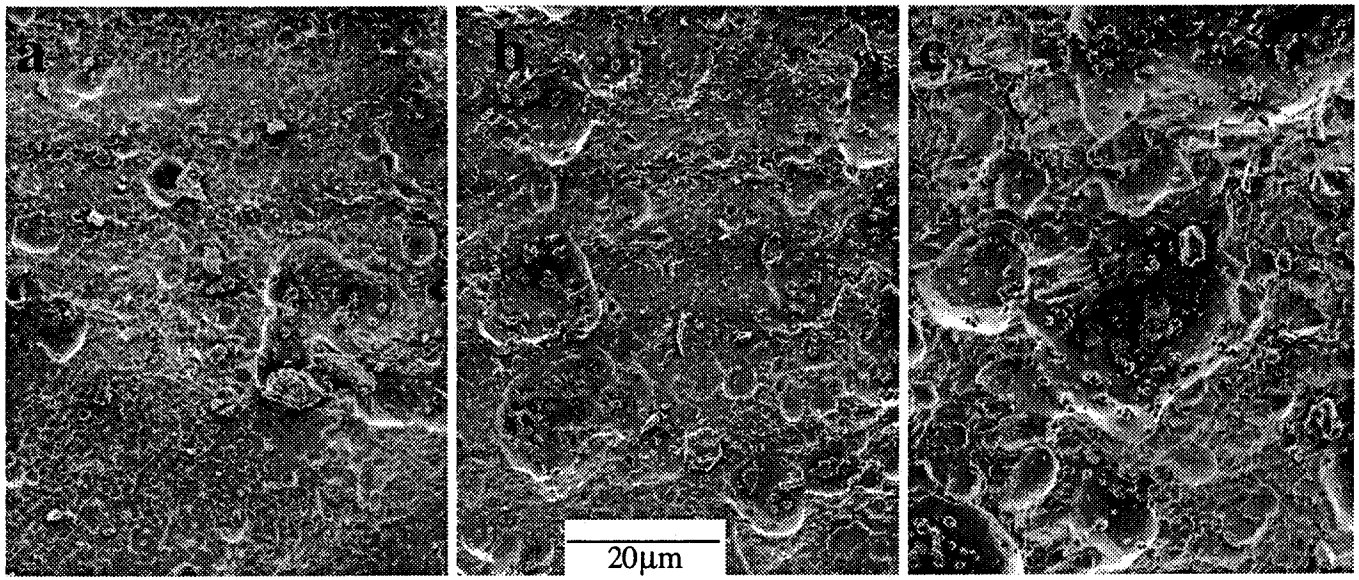

Figure 15. SEM secondary electron images of the Y_2O_3-dispersed FAS metal surface after oxidation at 1200°C in O_2 for (a) 100h (b) 200h and (c) 400h. The void fraction (smooth areas) increased with oxidation time.

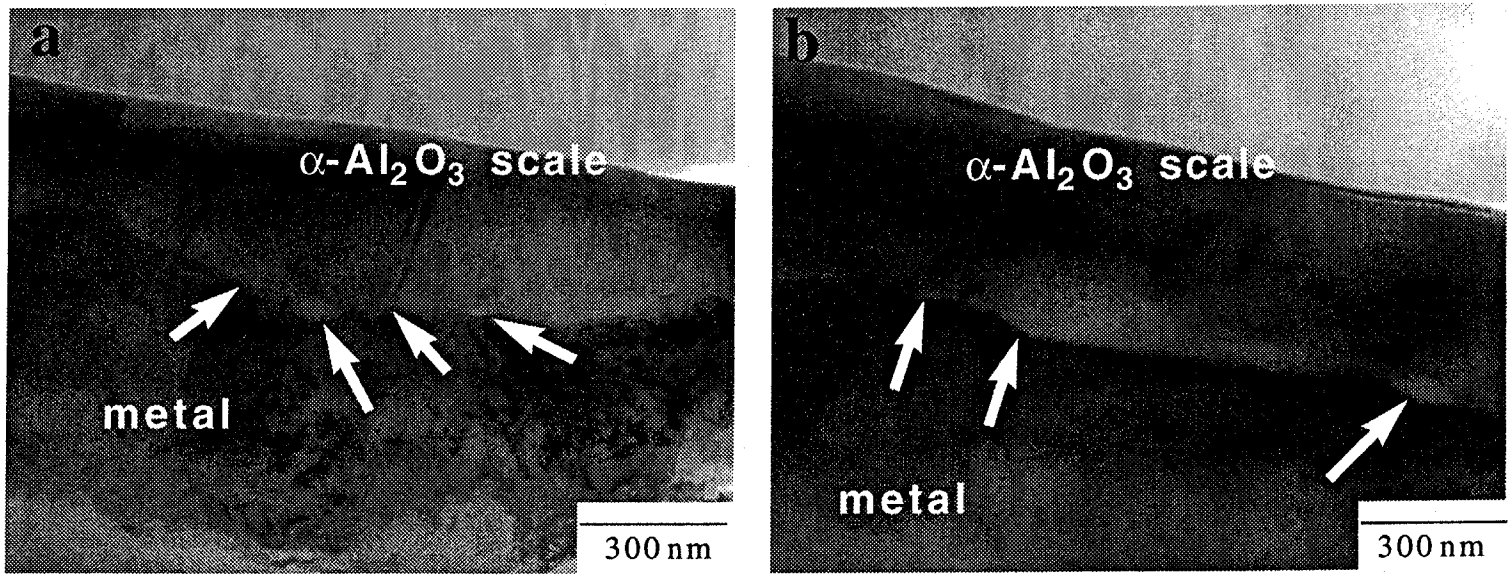

Figure 16. TEM bright field image of the metal-scale interface of Y_2O_3-dispersed Fe-28Al-2Cr after 2h at 1200°C in O_2. The arrows mark interfacial voids [35].

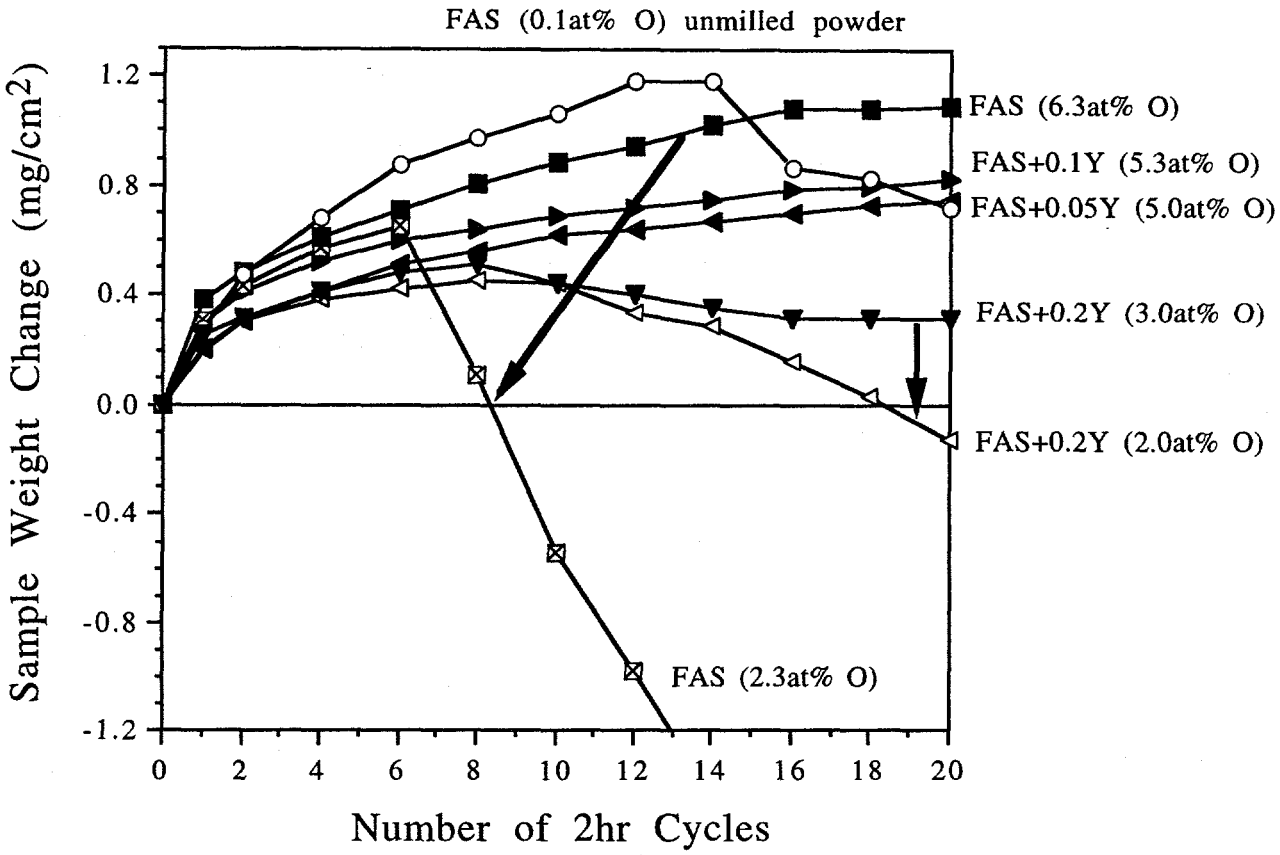

Figure 17. Sample weight change of Fe-28Al-2Cr (FAS) with various cation oxide dispersions cycled from room temperature to 1200°C with a cycle time at temperature of 2h. A larger amount of spallation was observed when the O content was reduced.

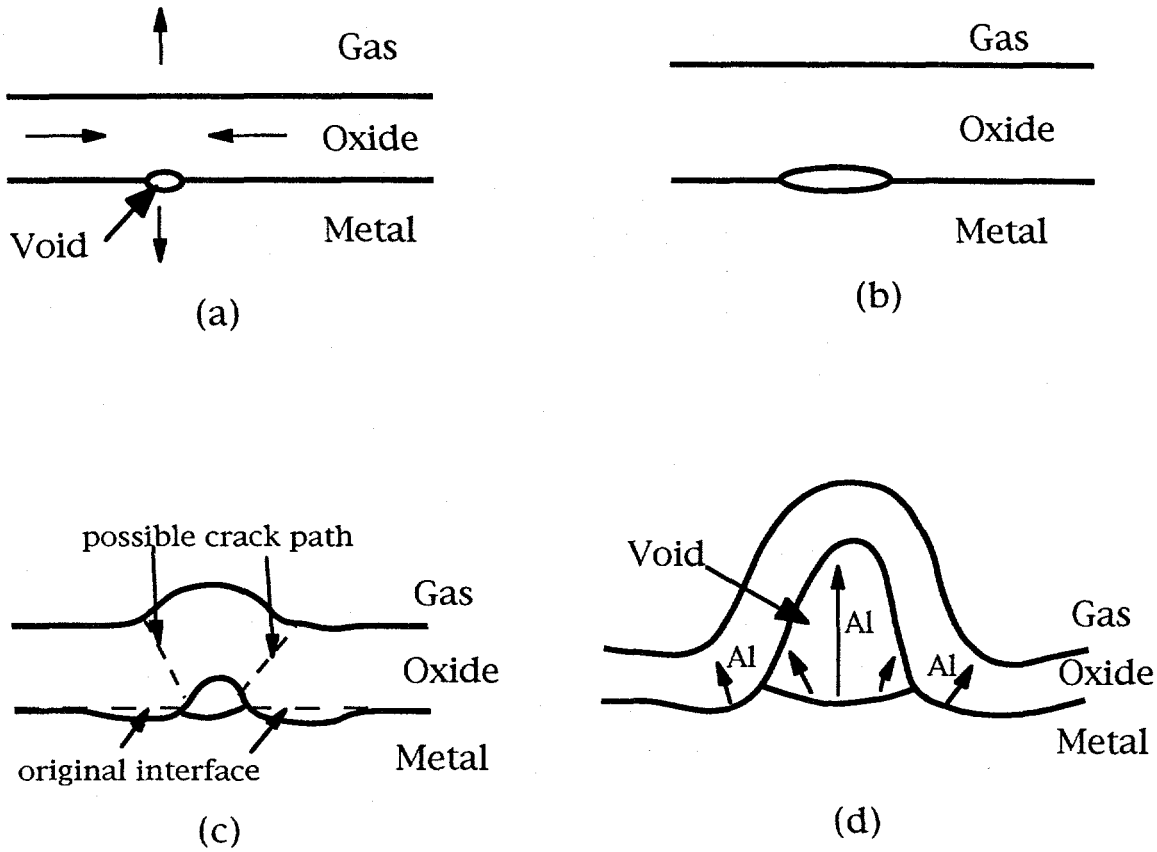
Gas
Oxide
Void
Metal
(a)
Gas
Oxide
Metal
(b)
possible crack path
Gas
Oxide
original interface
Metal
(c)
Void
Al
Al
Al
Gas
Oxide
Metal
(d)

Figure 18.